# Comparison of transceive endorectal and external surface array coils for prostate imaging at 7 Tesla

**G. J. Metzger[1], C. J. Snyder[1], C. Akgun[1], and G. Adriany[1]**

[1]Center for Magnetic Resonance Research, University of Minnesota, Minneapolis, MN, United States

**INTRODUCTION:** As for other anatomies, the availability of higher static magnetic fields increases the signal to noise (SNR) for imaging and spectroscopy studies in the prostate. Some researchers and clinicians have used the increased SNR at 3T as compared to 1.5T to focus on the sole use of an external surface array coil (SAC) as opposed to an internal endorectal coil (ERC) or an SAC combined with an ERC. The comparison of SAC and ERC advantages and disadvantages at ultra high field (UHF) require additional considerations above those previously considered. Unlike lower field strengths, UHF systems, such as the 7T used in these studies, typically do not employ the use of whole body RF transmit coils as prevalent on 1.5 and 3.0T scanners due to the increased power requirements and SAR considerations. Therefore, the SAC and ERC used at UHF must transmit and receive RF. The transmit/receive (T/R) characteristic of these coils has implications not only for SNR and receive B1 (B1-) homogeneity but also on required power and transmit B1 (B1+) homogeneity. Two different coil configurations are compared in this paper with respect to several of these factors, an external 16 channel stripline SAC and a single loop ERC.

**METHODS:** The MRI systems used for this study included a Magnex 7T, 90cm bore magnet with Siemens console and whole body gradients. For transmitting with the SAC, a series of 16, 1 kW amplifiers with independent phase and gain control were used (CPC, Pittsburgh, PA). Power monitoring was performed by Siemens hardware on a single channel and by in-house hardware and software for all channels, to ensure that FDA limits on specific absorption rates (SAR) were not exceeded. The transceiver SAC was a flexible 16 channel stripline TEM design with 8 elements mounted on both anterior and posterior flexible PTFE plates [1]. An automated version of the subject dependent B1+ shimming presented previously was performed to optimize transmit efficiency and homogeneity in a region around the prostate [2].
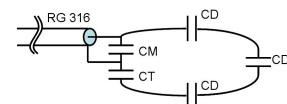


Fig. 1: Schematic diagram of the ERC. With the positions of the matching (CM), tuning (CT) and distributed (CD) capacitance.

The endorectal coil used in this study was similar to that first demonstrated by Klomp et al. as being safe for in vivo imaging at 7 Tesla [3]. This coil was built using the housing of a commercial 3T balloon-type endorectal design (BPX-30, Medrad, Pittsburgh, PA) with modified circuitry to match to 50 Ω at 297 MHz. In addition, we implemented two additional capacitive shortenings with a final loop size of approximately 3.5cm in width and 7cm in length (Fig. 1). The balloon of the ERC was filled with a perfluorocarbon (Fluorinert, 3M, St. Paul, MN) to minimize susceptibility effects. Benchtop and experimental data were acquired on a saline phantom prior to in vivo studies to verify coil performance and safety. Finite difference time domain (FDTD) modeling was also performed to simulate transmit B1 fields for comparison with measured data (REMCOM, State College, PA).

Imaging data was collected on a healthy volunteer with both coils under an IRB approved protocol. Anatomic T2w turbo spin echo (TSE) images were acquired with identical sequences to qualitatively assess image quality and to quantitatively determine SNR (TR 3050 ms, TE 130 ms, turbo factor 9, slice thickness 3 mm, FOV 280 mm, matrix 320x314, slices 10-20, resolution 0.7x0.7x3.0 mm$^3$). SNR was determined from these acquisitions from the peripheral zone and central gland by manually tracing these clearly visible regions.

**RESULTS:** Simulations of the coil in Fig. 1 provided insight into the expected B1+ profile of the ERC used in this study. Fig. 2a shows the relative simulated B1+ distribution which is characteristically asymmetric. The B1+ field was then measured experimentally with a two flip angle method in a gel phantom. The measured field map, Fig 2b, is in good agreement with the simulated results as demonstrated by the horizontal and vertical profiles in Figs. 2c and 2d respectively. The target flip angle in this study was 45 degrees which was achieved at a distance of 2.5 cm from the loop coil when using a reference voltage of 50 V (i.e. the RMS voltage required to achieve a 90 flip angle with a 500 ms RF pulse).
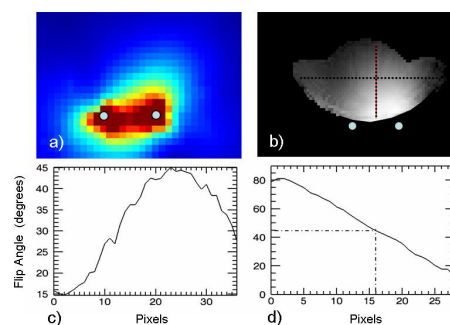


Fig. 2: (a) Simulated ERC B1+. (b) Measured B1+ map of the ERC with horizontal (c) and vertical (d) profiles. The blue dots in (a) and (b) represent the cross section of the loop conductor of the ERC.

In vivo imaging was initially performed with the 16 channel stripline after B1+ shimming which is necessary to maximize transmit efficiency and homogeneity. A representative slice zoomed in on the prostate is shown in Fig. 3a from this dataset. The SNR in both the peripheral zone (SNRp) and central gland (SNRc) were determined: SNRp = 45 and SNRc = 37. On a separate day, ERC imaging was performed on the same subject. The large B1+ inhomogeneity accompanying a transceive ERC cannot be corrected with B1+ shimming therefore imaging was performed at several different power levels making sure not to exceed FDA limits for local SAR. The TSE data acquired for Fig. 3b was acquired with 4 times the power as Fig. 3c. While improving the SNR and contrast in regions of the prostate far from the coil, close to the coil the B1+ results in overflipping of the spins, Fig 3b. With a more modest power setting in Fig. 3c, the peripheral zone has a higher SNR over Fig. 3b but the central gland and contrast is lost anteriorly. However, in both cases there is over a 6 fold SNR increase in the peripheral zone with the ERC compared to the external surface array (SAC). As expected, SNR improvements in the central gland were lower due to this anatomies distance from the ERC. Finally, initial attempts and improving resolution were also attempted, Fig. 4. These data were acquired with the lower of the two power settings and demonstrate that even with minor improvement of in-plane resolution the margins and structures of the prostate become more apparent.
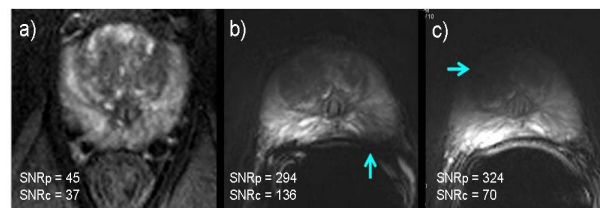


Fig. 3: Comparison of the same T2w TSE acquisition with the SAC (a) and the ERC at a higher (b) and lower (c) power setting. SNR figures for the peripheral zone (SNRp) and central gland (SNRc) are given for each image. The blue arrows indicate excessive B1+ (b) and weak B1+ (c) due to transmit power settings.

**DISCUSSION:** This is the first reported comparison of an SAC and ERC for anatomical imaging of the prostate at 7 Tesla. These results, demonstrate that the promise of improved spatial resolution at increased field strengths will continue to be realized at 7 Tesla for the prostate. However, a comprehensive study investigating both SNR and achievable resolutions in comparison with lower field strength systems needs to be undertaken before any definitive statements can be made in this regard. While it is tempting to trade the increased SNR at 7T for a SAC type approach to prostate imaging, there are many obvious advantages to the use of an ERC even at 7T as evident from the anatomic imaging results obtained in this study.
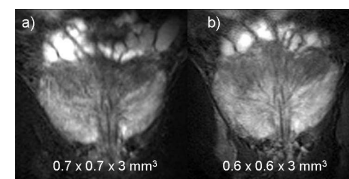


Fig. 4: Coronal T2W TSE images of the prostate with an ERC.

**REFERENCES:** [1] Snyder et al. ,Proceedings of the 15th Annual Meeting of ISMRM, Berlin, Germany, 2007 p 164. [2] Metzger et al. Local B1+ shimming for prostate imaging with transceiver arrays at 7 based on subject-dependent Transmit Phase Measurements, MRM (In Press) [3] Klomp et al. Proton spectroscopic imaging of the human prostate in vivo at 7T, Proceedings of the 6th bi-annual Minnesota Workshops, 2007.